



PAPER • OPEN ACCESS


Li-doped transition metal high-entropy oxides (Li/TM-HEOs) as Li-Ion batteries cathodes: a first report on capacity fading and cycling stability

To cite this article: Luca Spiridigliozzi *et al* 2024 *Mater. Res. Express* 11 045504View the [article online](#) for updates and enhancements.

You may also like

- [Effects of helium implantation on mechanical properties of \$\(Al_{0.34}Cr_{0.26}Fe_{0.14}Ni_{0.35}\)O\$ high entropy oxide films](#)
Zhao-Ming Yang, , Kun Zhang et al.
- [Localisation of vibrational modes in high-entropy oxides](#)
C M Wilson, R Ganesh and D A Crandles
- [High entropy materials as emerging electrocatalysts for hydrogen production through low-temperature water electrolysis](#)
Jonathan Ruiz Esquiú and Lifeng Liu

Breath Biopsy Conference

 5th & 6th November
OnlineBREATH
BIOPSY

Join the conference to explore the **latest challenges** and advances in **breath research**, you could even **present your latest work!**


Register now for free! Main talks Early career sessions Posters

Materials Research Express



PAPER

Li-doped transition metal high-entropy oxides (Li/TM-HEOs) as Li-Ion batteries cathodes: a first report on capacity fading and cycling stability

OPEN ACCESS

RECEIVED
25 November 2023

REVISED
4 March 2024

ACCEPTED FOR PUBLICATION
21 March 2024

PUBLISHED
5 April 2024

Original content from this work may be used under the terms of the [Creative Commons Attribution 4.0 licence](#).

Any further distribution of this work must maintain attribution to the author(s) and the title of the work, journal citation and DOI.



Luca Spiridigliozzi¹, Andrea Filippo Di Feo¹, Grazia Accardo², Uxue Gonzalez Mendizabal², Emanuele Di Bona³ and Gianfranco Dell'Agli^{1,4}

¹ Department of Civil and Mechanical Engineering, University of Cassino and Southern Lazio, Via G. Di Biasio 43, 03043 Cassino (FR), Italy

² Centre for Cooperative Research on Alternative Energies (CIC energiGUNE), Basque Research and Technology Alliance (BRTA), Alava Technology Park, Albert Einstein 48, 01510, Vitoria-Gasteiz, Spain

³ Department of Industrial Engineering, University of Trento, Via Sommarive 9, 38123 Trento, Italy

⁴ INSTM—National Interuniversity Consortium of Materials Science and Technology, Via G. Giusti 9, 50121 Florence, Italy

E-mail: gianfranco.dellagli@unicas.it

Keywords: high-entropy oxides, Li-Ion Batteries, Co-precipitation, NMR, Cyclic voltammetry

Abstract

High-Entropy Oxides (HEOs) have gained significant attention for their wide range of compositions and potential applications across various sectors, including rechargeable batteries. This study explores the characterization of two distinct HEO systems as potential cathode materials for Lithium-ion batteries (LIBs). A series of rock salt structured HEOs with varying Li loadings (16Li/RS-HEO, 25Li/RS-HEO, 33Li/RS-HEO, and 41Li/RS-HEO) and a spinel-structured HEO with 16 mol% of Li loading (16Li/SP-HEO) were firstly synthesized through co-precipitation. Electrochemical analyses via cyclic voltammetry revealed stark differences in the behavior of these structures. The Li/SP-HEO sample displayed broad and strongly irreversible hysteresis cycles, while the Li/RS-HEO series manifested thin, narrow hysteresis cycles with single oxidation peaks between 0.5 V and 0.7 V. As the lithium content increases in the RS-HEO system, the cycling stability of the cell decreases, most likely due to the reduced ratio of transition metal cations to lithium ions. Although there was a noticeable decrease in capacity under higher current rates, the higher lithium loadings positively impact the cell capacity, albeit with notable capacity fading under higher current rates. Li-doped rock salt structured high entropy materials show potential for LIB cathodes in terms of high specific capacities; the observed stability issues at medium and high current densities indicate a rapid electrode degradation.

1. Introduction

High-Entropy materials represent a relatively recent category of materials, uncovered through two independent studies in 2003/2004 on the equimolar composition of a (FeCrMnNiCo) alloy, forming a singular FCC (Face-Centered Cubic) solid solution [1, 2].

Approximately a decade later, in 2015, Rost *et al* groundbreaking work [3] expanded the 'high-entropy concept' to ceramic materials by successfully synthesizing a rocksalt single-phase oxide: $(\text{Co}_{0.2}\text{Ni}_{0.2}\text{Mg}_{0.2}\text{Zn}_{0.2}\text{Cu}_{0.2})\text{O}$, and demonstrating its reversible behaviour at about 700 °C–800 °C. Specifically, in Rost's work, it has been shown that entropy governs the transition from a system with multiple phases to a single-phase system. This occurs when the positive entropic contribution exceeds the positive enthalpy of formation at a specific temperature, leading to a negative free energy of formation ($\Delta G_f = \Delta H_f - T\Delta S_f$). This transition, which happens at a particular temperature determined by the interplay between entropy and enthalpy in each specific system, is endothermic and reversible.

Since then, further studies [4–8] have continuously extended the synthesis to other subclasses of High Entropy Ceramics (HECs), each one exhibiting peculiar and often unexpected properties [9–12], as well as improving the technological process of their production [13, 14].

The growing interest in High Entropy Oxides (HEOs) is mainly due to their ability to create infinite combinations of properties and compositions. This is achieved by adjusting the interactions between the different elements involved within the entropy-stabilized lattice. Recently, several HEOs have demonstrated unique and promising functional properties such as dielectric properties [15], high-temperature stability and sintering resistance [16, 17], exceptionally low thermal conductivities [18], magnetic [12] and electrochemical properties [15].

Broadly, the electrochemical behavior of HEOs can be virtually customized by altering their elemental composition. With the availability of a wide range of crystal structures, cations, and combinations, HEOs offer an exceptional opportunity to design and engineer new functional materials. Particularly, rock salt and spinel-like crystal structures have shown promise for various energy applications, ranging from conversion to storage [10, 19–21].

Meeting the increasing demand for energy storage, from handheld devices to electric mobility and stationary applications, the development of rechargeable batteries based on Li represents one of the most significant challenges in the energy sector. One of the most crucial objectives in such a sector is the development of next-generation batteries that demonstrate longevity, high rates, and substantial reversible specific capacities. Thus, the quest for high-performing materials (primarily anode and cathode materials) for next-generation batteries stands out as a research priority of critical interest for the entire scientific community [22, 23].

Given their unique properties, High-Entropy Ceramics are regarded as a compelling new class of materials in the field of Li-based batteries, at least from the first studies available till now [24–26]. More specifically, High Entropy Fluorides (HEFs) constitute an enticing category of materials for cathodes due to their heightened electronegativity, substantial theoretical capacity (approximately 600 mAh g^{-1}), and sufficient cycling stability [27].

High Entropy Oxides (HEOs) offer superior Li conductivity [11] and multiple electrochemically active components compared to single metal oxides. Furthermore, they partially mitigate the hazardous effects instigated by forming Solid Electrolyte Interphases (SEIs) and dendrites within the cell, thus possibly addressing the problem of electrode pulverization [28, 29].

Finally, as the most widely distributed Li-ion batteries (LIBs) available on the market are based on both cobalt oxides and their derivatives and nickel oxides and their derivatives, the high compositional flexibility of HEOs can help in strongly diluting the use of Co and Ni in LIB cathodes.

Our study presents a pioneering study in the field of lithium-ion batteries (LIBs), introducing an innovative approach to cathode material design using differently structured lithium-doped high-entropy oxides (Li-HEOs). By doping HEOs with lithium, an enhancement of the intrinsic electrochemical characteristics of the cathode is expected, potentially leading to LIBs with improved energy density and/or cycling stability [30, 31]. However, their exploration in the realm of LIB cathodes is at its beginnings and somewhat contradictory [28, 32].

In this context, the present work aims at investigating the structural and electrochemical properties of two differently structured HEOs used as novel LIBs cathodes: a rock salt one with different Li loading (16 mol%, 25 mol%, 33 mol% and 41 mol% – 16Li/RS-HEO, 25Li/RS-HEO, 33Li/RS-HEO, 41Li/RS-HEO, respectively) and a spinel-like one with 16 mol% of Li loading ($(\text{Li}_{0.167}\text{Mn}_{0.167}\text{Ni}_{0.167}\text{Co}_{0.167}\text{Zn}_{0.167}\text{Fe}_{0.167})_3\text{O}_{4-\delta}$ – 16Li/SP-HEO).

Finally, the cycling stability and the capacity retention (or fading) of the assembled LIBs are discussed to better understand the feasibility of High-Entropy Oxides as potential cathode materials for next-generation Lithium-ion batteries, especially in terms of capacity fading.

2. Materials and methods

Zinc (II) nitrate hexahydrate ($\text{Zn}(\text{NO}_3)_2 \cdot 6\text{H}_2\text{O}$, Sigma Aldrich), Copper (II) nitrate trihydrate ($\text{Cu}(\text{NO}_3)_2 \cdot 3\text{H}_2\text{O}$, Sigma Aldrich), Nickel (II) nitrate hexahydrate ($\text{Ni}(\text{NO}_3)_2 \cdot 6\text{H}_2\text{O}$, Sigma Aldrich), Cobalt (II) nitrate ($\text{Co}(\text{NO}_3)_2 \cdot 5\text{H}_2\text{O}$, Carlo Erba Reagents), Magnesium (II) nitrate ($\text{Mg}(\text{NO}_3)_2 \cdot 5\text{H}_2\text{O}$ RPE, Carlo Erba Reagents), Iron (II) sulfate heptahydrate ($\text{Fe}(\text{SO}_4) \cdot 7\text{H}_2\text{O}$, Carlo Erba Reagents), Manganese (II) nitrate hydrate ($\text{Mn}(\text{NO}_3)_2 \cdot \text{H}_2\text{O}$, Carlo Erba Reagents) were used as precursors for preparing the aqueous solutions used to synthesize the two equimolar HEO systems (RS-HEO and SP-HEO). The purity of all precursor salts was $\geq 99\%$.

They have been synthesized via co-precipitation by using NaOH (Sodium Hydroxide, pellets, Carlo Erba Reagents) as a precipitating agent, as a highly alkaline environment has to be maintained to prevent an incomplete Mg precipitation, and ammonia should be avoided to prevent the formation of undesired complexes in the Cu-containing system [33].



Figure 1. Example of the as-prepared 16Li/SP-HEO cathode.

A typical co-precipitation synthesis, used for both RS-HEO and SP-HEO systems, firstly involved the dissolution of the proper amount of precursor salts in de-ionized water to obtain a solution (solution A) with a total cation concentration of 0.1 M (so that each cation has a concentration of 0.02 M). Parallely, a dissolution in a separate beaker of sodium hydroxide (NaOH) in de-ionized water to obtain a 1 M solution (solution B) has been carried out. Subsequently, solution A has been added to solution B, keeping it under vigorous stirring. The as-obtained gelatinous co-precipitate has been filtered and washed with de-ionized water. Finally, the filtered and washed co-precipitate has been dried overnight at 60 °C.

The Li impregnation of the as-synthesized samples involved dissolving a proper amount of lithium nitrate (LiNO_3 , Carlo Erba Reagents, purity $\geq 99\%$) in deionized water and subsequently introducing the powdered substrate (alternatively RS-HEO or SP-HEO) to such solution. The resulting suspension is then thoroughly mixed using a magnetic stirrer and subjected to heating, thus facilitating the gradual evaporation of water, leading to the steady and homogeneous precipitation of lithium nitrate. Ultimately, this process results in a uniform dispersion of the precipitated compound particles within the substrate [34–37].

As already reported in the literature and observed for very similar systems [38], a significant loss of lithium due to the impregnation process to add it within the HEO system is always present and predictable in the measure of around 30%. Thus, we used such excess of lithium precursors in our synthesis to overcome this predictable loss. Based on those considerations, we could suppose that the nominal Lithium content is still present within the differently fabricated cathodes.

The resulting Li/RS-HEO and Li/SP-HEO systems have been subsequently calcined by using the following thermal cycle: from room temperature to 300 °C (10 °C min^{-1} as heating rate), soaking at 300 °C for 2 h, from 300 °C to 650 °C (10 °C min^{-1} as heating rate), soaking at 650 °C for 1.5 h, from 650 °C to 1100 °C, soaking at 1100 °C for 1.5 h, air-quenching from 1100 °C to room temperature.

A structural analysis was carried out by XRD (Panalytical X'PERT MPD diffractometer, Cu K α radiation) on both undoped and Li-doped RS-HEO and SP-HEO powders.

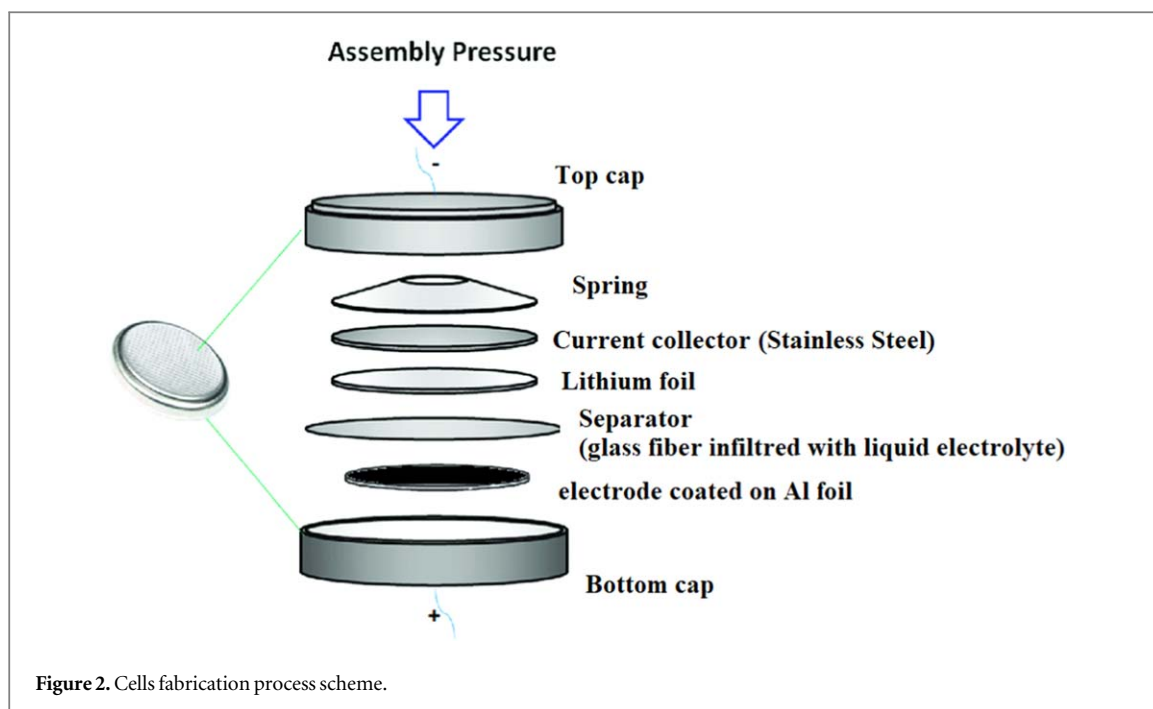
TG/DTA analysis was performed in air using a heating rate of 10 °C min^{-1} and $\alpha\text{-Al}_2\text{O}_3$ as a reference with a Netzsch Thermoanalyzer STA 409.

Solid-state NMR analysis was carried out on the Li/RS-HEO powders with a Bruker 400WB spectrometer operating at a proton frequency of 400.13 MHz. All the samples were weighted before the analysis to rescale the related spectrum.

Scanning Electron Microscopy measurements and chemical analysis by electron-dispersive spectroscopy (EDS) of the various samples were carried out by using 'QUANTA 200FEG' Thermo Fischer.

2.1. Cathodes and cells preparation

To produce the different HEO cathodes, inks were made using powdered active materials (i.e. 16Li/RS-HEO, 25Li/RS-HEO, 33Li/RS-HEO, 41Li/RS-HEO and 16Li/SP-HEO). The inks had a composition of 80% active material, 10% carbon C65, and 10% polyvinylidene fluoride (PVDF) in a 2% weight solution of N-Methyl-2-pyrrolidone (NMP). Firstly, PVDF was dissolved in NMP with overnight stirring. Once dissolved, C65 was added to the corresponding quantity of 2 wt% PVDF-NMP and mixed in an IKA stirrer for 5 min at a speed of 16000 rpm. The cathode active material was then added to the mixture and stirred for an additional 5 min at 16000 rpm. The prepared ink was allowed to rest for 1 h in a ball miller to remove as many bubbles as possible before being spread on aluminium foil using a Doctor Blade (RK control coater) with a blade thickness of 500



microns. The laminates were then dried at room temperature in air for 2 h and subsequently at 80 °C for 12 h in a vacuum oven. Finally, the designed HEO cathodes were obtained approximately 120 microns thick. Active material loadings of different samples were the following:

- Li16/RS-HEO: 8.45 mg;
- Li25/RS-HEO: 8.06 mg;
- Li33/RS-HEO: 8.06 mg;
- Li41/RS-HEO: 11.67 mg;
- Li16/SP-HEO: 8.45 mg.

Given the area of the tested cells being 1,13 cm², active material's loading in cathode is (in average) 7,5 mg /cm². Figure 1 shows an example of the as-prepared 16Li/SP-HEO cathode).

For the manufacture of cells, cathodes of 12 mm diameter were cut. All assembly is carried out inside a glove box, with an inert atmosphere. The lithium disk used as a counter electrode is 14 mm, and both are separated by the separator (fibreglass) soaked in a few drops of LiPF₆ electrolyte.

The LiPF₆-based electrolyte employed in our study is a 1 M solution (sourced from Merck) of lithium hexafluorophosphate (LiPF₆) dissolved in a solvent mixture of ethylene carbonate (EC) and diethyl carbonate (DC), with the composition being an equal volume ratio of 50/50 (1 M LiPF₆ in EC/DEC 50/50 v/v).

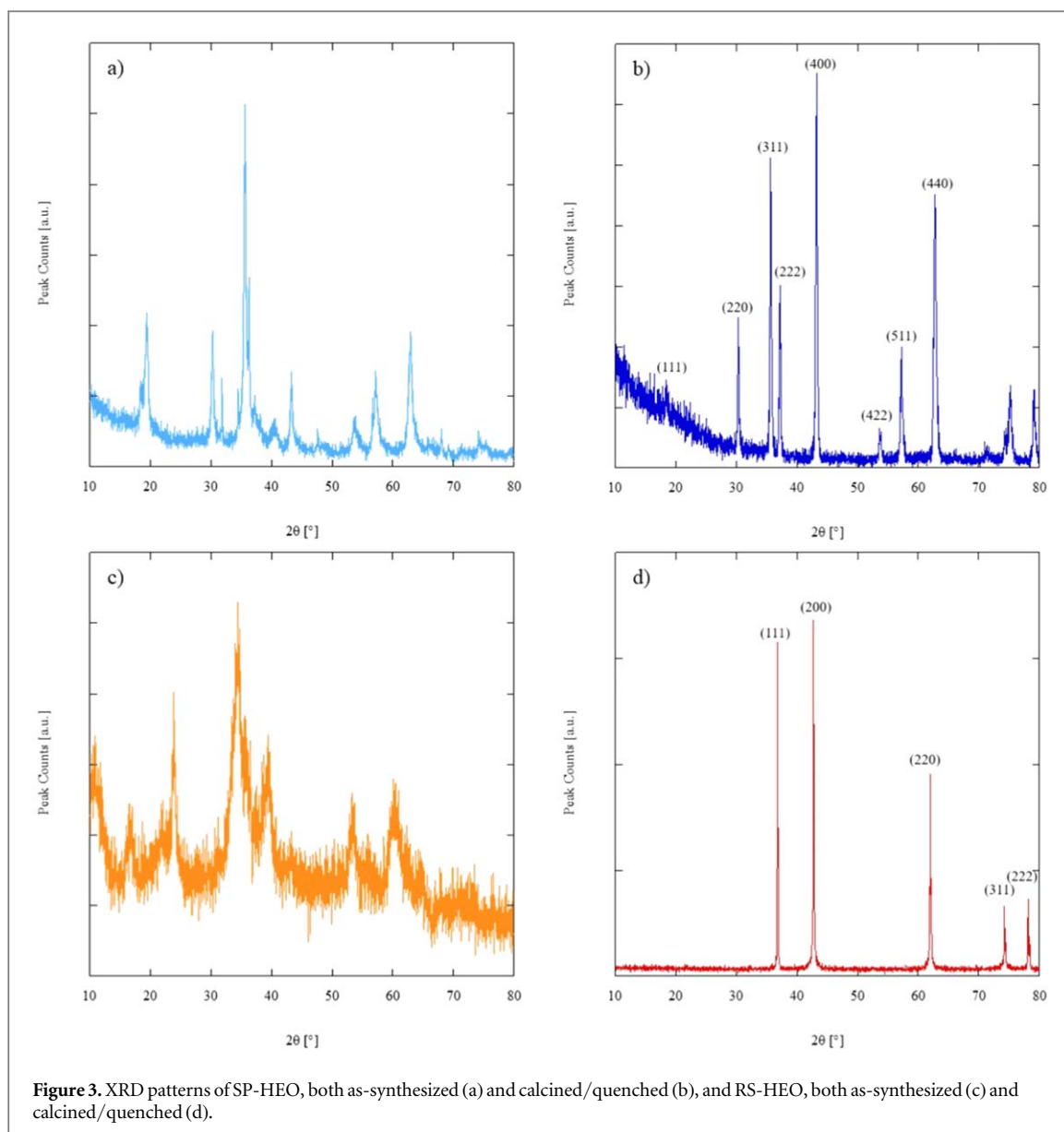
The entire system is then hermetically sealed. Figure 2 exemplifies such a cell assembly procedure.

The cell was connected to a 'Maccor series 4000 battery tester (Maccor Inc., USA)' and tested upon assembly. During the tests, a current flow was induced between the working and counter electrodes, and the applied potential was controlled by manipulating the polarization of the counter electrode. The potential is measured between the working electrode and the known stable potential of the reference electrode. Each tested cell performed several deeply charge–discharge cycles to evaluate its electrochemical response, by using the following current values: 50 mA/g, 100 mA/g, 200 mA/g, 500 mA/g, 750 mA g⁻¹, and 1000 mA/g.

3. Results and discussion

3.1. Configurational entropy estimation

Configurational entropy, i.e. S_{conf} is one of the most important features of an HEO. In the case of the Li0/RS-HEO, the proof of high entropy was reported in the pioneereristic work of Rost *et al* [3]; therefore, the addition of lithium in the rocksalt structure, in octahedral position [38] likely leads to a further increase of entropy.



Indeed, the calculation of S_{conf} in the ideal model by the well-known expression $R \sum x_i \ln(x_i)$ (see [3], for example) leads to:

- 0Li/RS-HEO: 1.61 R;
- 16Li/RS-HEO: 1.76 R;
- 25Li/RS-HEO: 1.77 R;
- 33Li/RS-HEO: 1.72 R;
- 41Li/RS-HEO: 1.63 R

Thus, our calculations show that for each Li-doped RS-HEO sample, ΔS_{conf} is well greater than the threshold proposed in the literature to define an HEO (i.e. $S_{\text{conf}} \geq 1.5 R$).

The determination of S_{conf} is much more complex in the case of spinel, as the presence of two cationic sites requires the knowledge of cationic distribution among them. Based on such cationic distribution, Sarkar [39] calculated S_{conf} for a system similar to one of the present study but without lithium. To estimate the cationic distribution between octahedral and tetrahedral sites, we have used the results obtained by Sarkar [39]. Indeed, he found that Co is all in the tetrahedral sites, Mn and Ni are all in the octahedral sites, whereas Fe is partly in the octahedral (1/3) and partly in the tetrahedral site (2/3); we have used such results whereas for Li we have assumed that it occupies only octahedral sites (on the base of our previous result [38]) and finally the distribution

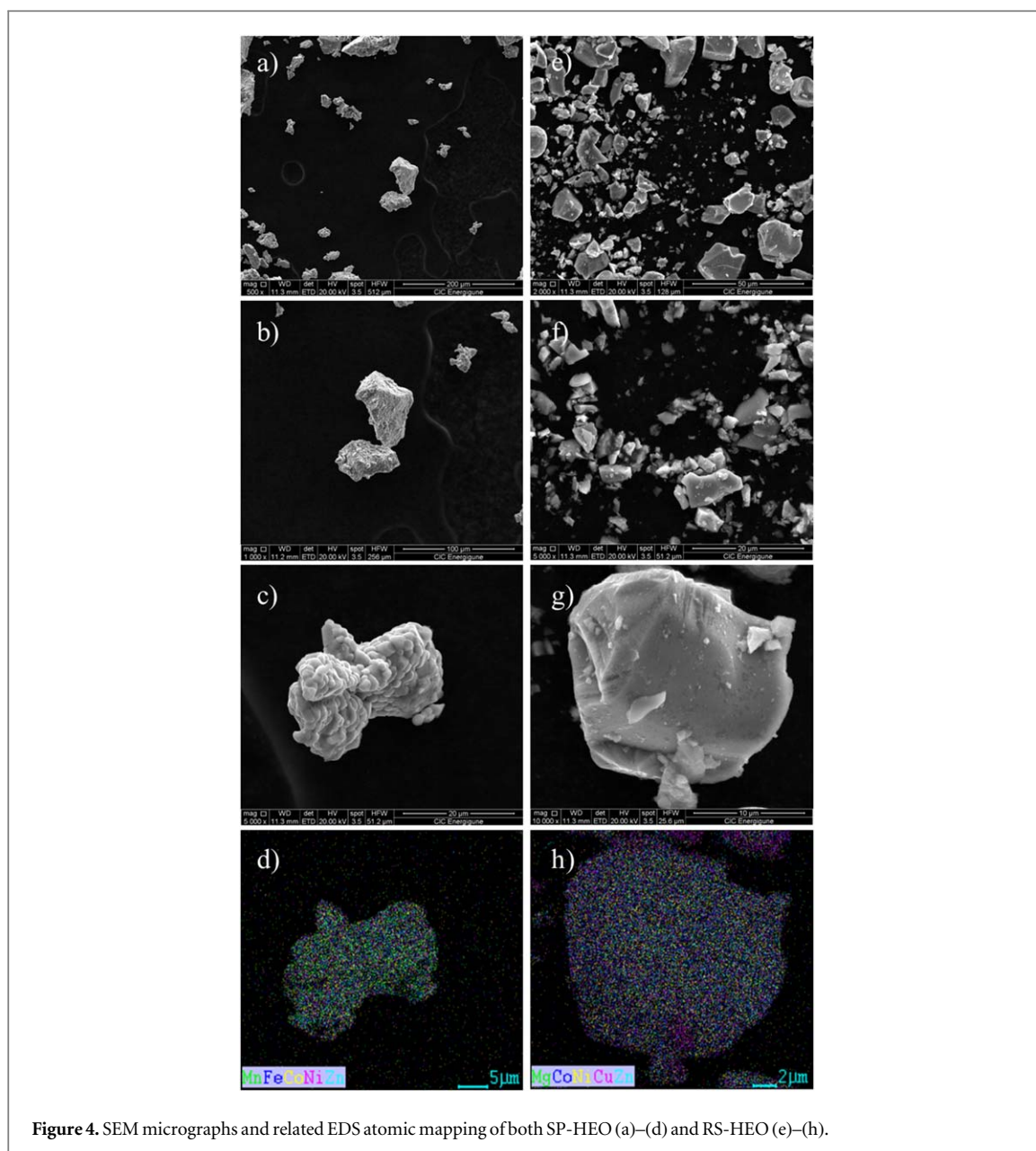
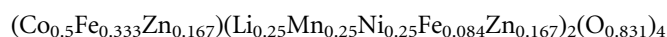


Figure 4. SEM micrographs and related EDS atomic mapping of both SP-HEO (a)–(d) and RS-HEO (e)–(h).

of Zn is derived from the ratio of tetrahedral and octahedral sites occupation in spinel and inverse spinel structure (i.e. 1:2), leading to this chemical formula:



The Oxygen coefficient has been estimated by using again the results of Sarkar [39] for the oxidation state of Fe (+3), Co (+2.4), Mn (+2.9) and Ni (+2), whereas we have assumed for Li and Zn, as oxidation states, +1 and +2 respectively. Under these hypotheses and applying the procedure reported in [39] (equations 1–5) we have obtained:

$$S_{\text{conf}} = 1.57R$$

This value, greater than 1.5 R, ensures that, under the indicated hypotheses, the synthesized spinel is actually an HEO.

3.2. Structural/microstructural characterization

Figure 3(a) shows the XRD pattern of the as-synthesized SP-HEO, exhibiting a combination of a spinel-like phase (Fe_3O_4 , ICDD Card n. 01-075-6109) and several different secondary phases attributable to ZnO (ICDD Card n. 01-070-2551), MnO (ICDD Card n. 01-075-0625), and cobalt hydroxide (ICDD Card n. 01-089-8616). Nevertheless, the presence of NiO cannot be excluded since it shares the same rocksalt structure as MnO, and its

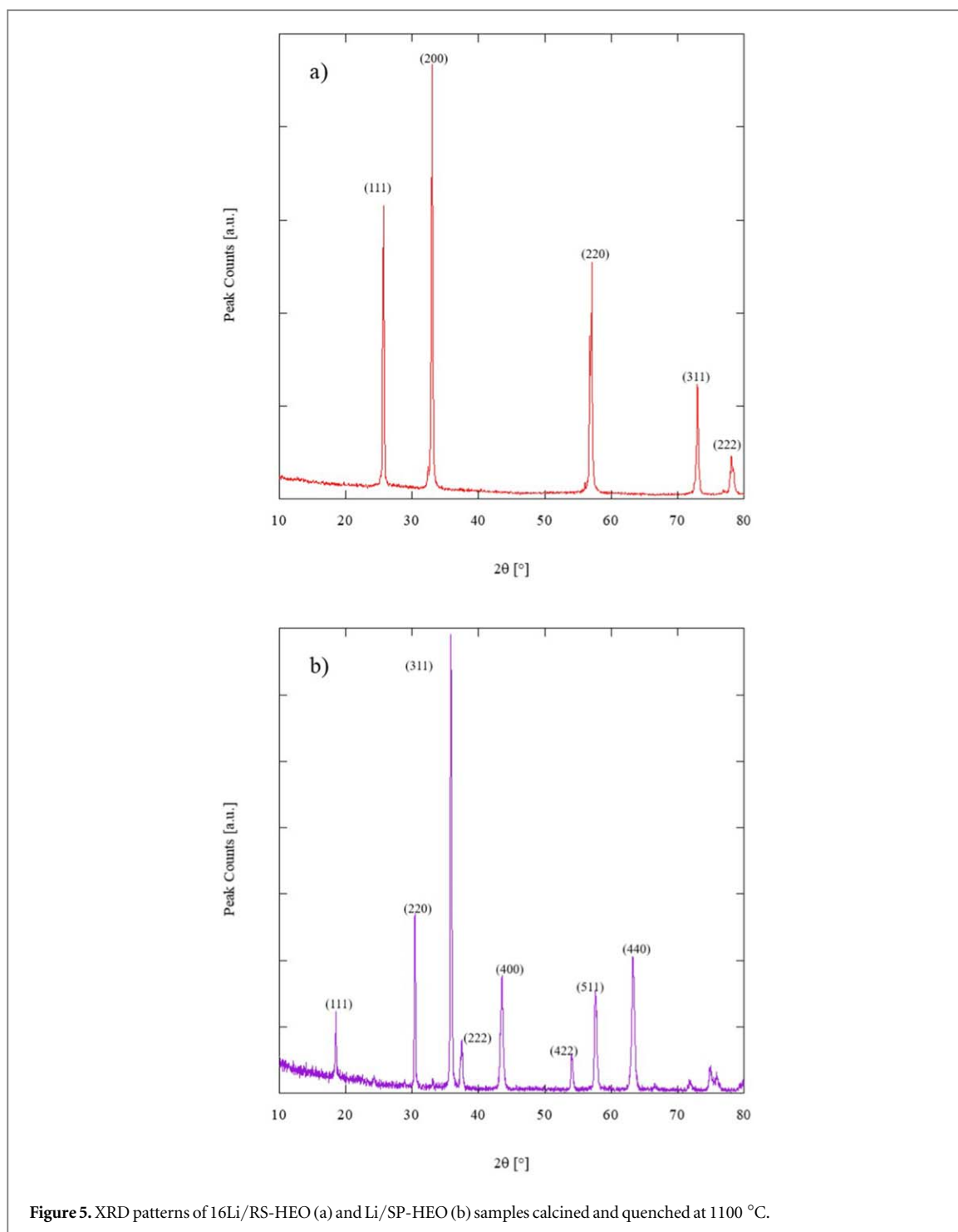


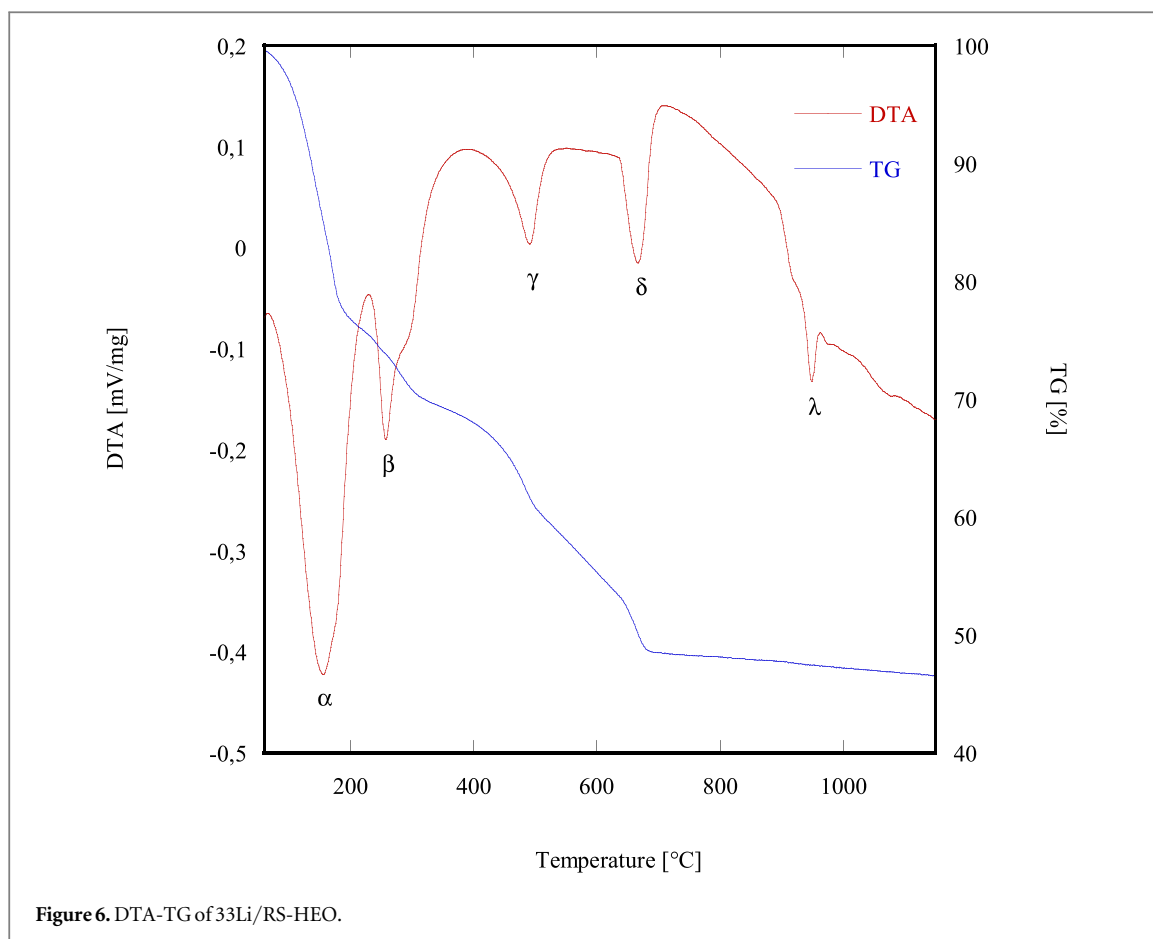
Figure 5. XRD patterns of 16Li/RS-HEO (a) and Li/SP-HEO (b) samples calcined and quenched at 1100 °C.

main peaks could overlap with those associated with MnO (being very broad and still partially overlapping with the main Fe_3O_4 reflections).

Indeed, the XRD pattern of SP-HEO calcined (and quenched) at 1100 °C, shown in figure 3(b), mainly exhibits a single-phase spinel-like structure (ICDD Card n. 01-089-3854).

Conversely, the as-synthesized RS-HEO (shown in figure 3(c)) only exhibits some very broad peaks, indicating its nanocrystalline nature along with an amorphous phase. Again, after calcination (and quenching) at 1100 °C for 1 h, RS-HEO (with no impregnated Li) owns an entropy-stabilized rocksalt structure (ICDD Card n. 01-075-0418), as evident in its diffraction pattern of figure 3(d).

Therefore, once single-phase HEO was obtained for both rocksalt and spinel structure materials, the detailed study of phase evolution as a function of the calcination temperature was not carried out in the present work. Indeed, on the one hand, in the case of RS-HEO, that study is already present in the literature [3, 33] even when doped with Li^+ [38]. On the other hand, the main focus of the present research was the electrochemical



characterization of different HEOs doped with Li^+ as possible electrodes for LIBs and not unravelling the intricate transformations leading to the entropy-stabilized single phase.

The lattice parameter of calcined/quenched RS-HEO (figure 3(d)) is 0.41981 nm, whereas the lattice parameter of calcined/quenched SP-HEO (figure 3(b)) is 0.83185 nm. These values have been obtained by the least square procedure adopted in the software UnitCell [40].

The morphology of the samples RS-HEO and SP-HEO prior to Li impregnation and the corresponding elemental distribution were analyzed by SEM/EDS.

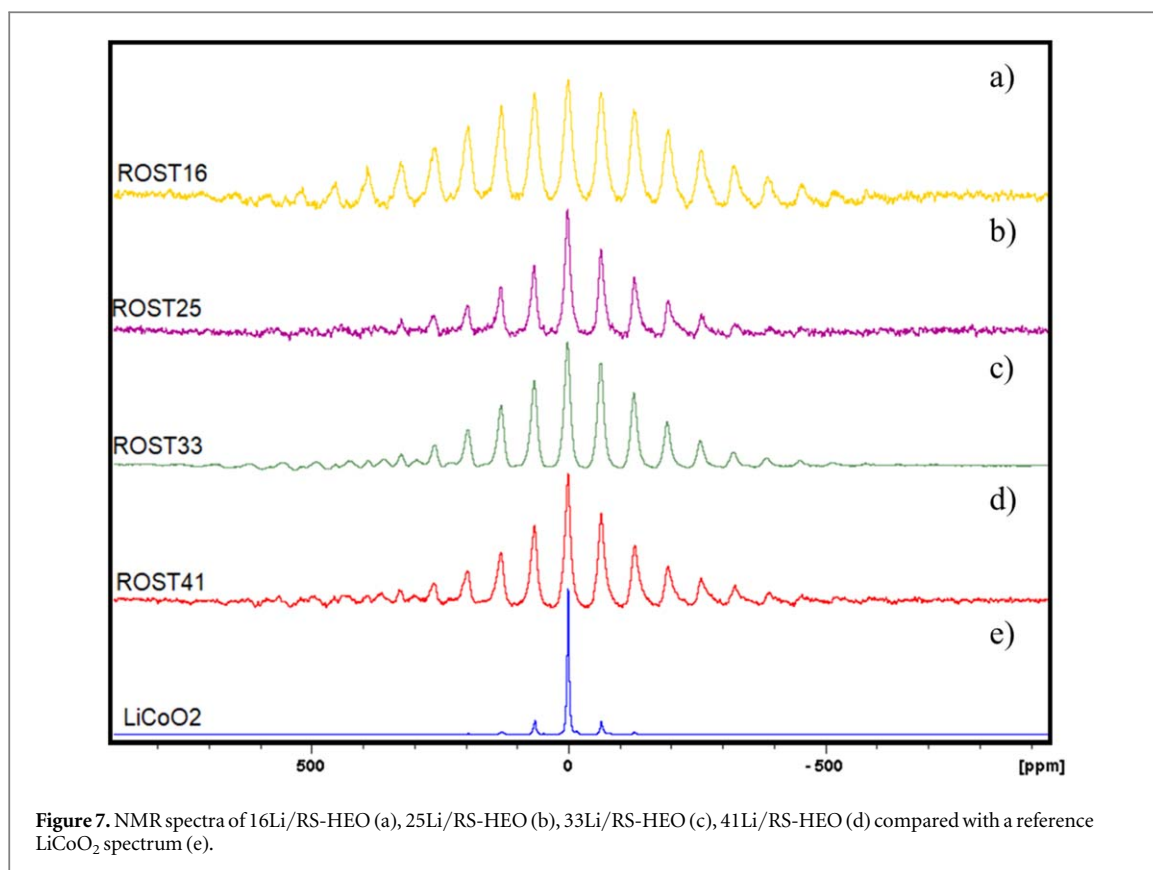
The micrographs in figure 4 reveal, for both samples, powders characterized by heterogeneous particle size and irregular shapes, with the presence of large agglomerates, whose size is in the order of tenths of μm . The presence of hard agglomerates is indeed evident in the micrographs at higher magnification (see figures 3(b), (c), (f) and (g)). This is an expected result considering the synthesis method and similar powder morphology is reported in the literature on both analogous and different chemical systems [41, 42], characterized by the presence of such hard agglomerates impairing their sinterability. However, being both RS-HEO and SP-HEO are intended as porous cathodes, it is believed that their final electrochemical behavior will benefit from such microstructural features.

Figures 4(d) and (h) shows the atomic mapping of RS-HEO and SP-HEO, revealing a highly homogeneous distribution of all cations, being an indirect confirmation of their entropy-stabilized single-phase structures (either rocksalt or spinel-like).

Prior to the cathode fabrication, both RS-HEO and SP-HEO were loaded with different Li contents (16 mol%, 25 mol%, 33 mol% and 41 mol% for the RS-HEO system, and 16 mol% for the SP-HEO system) by using the largely-used and well-known wet impregnation method [29, 30].

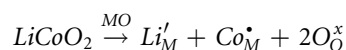
Research evidence has shown that approximately 30% of introduced lithium is lost during the 'wet impregnation' [38]. Therefore, for all the prepared cathode active materials (16Li/RS-HEO, 25Li/RS-HEO, 33Li/RS-HEO, 41Li/RS-HEO), the nominal quantity of lithium nitrate has been increased by 30%.

Figure 5 shows the XRD patterns of both 16Li/RS-HEO (exemplary for the Li/RS-HEO series) and Li/SP-HEO systems calcined (adopting the thermal cycle described in the Materials and Methods section, designed to ease a homogeneous lithium nitrate decomposition) and quenched at 1100 °C after 1.5 h, highlighting how the Li-impregnation did not alter their crystal structures.



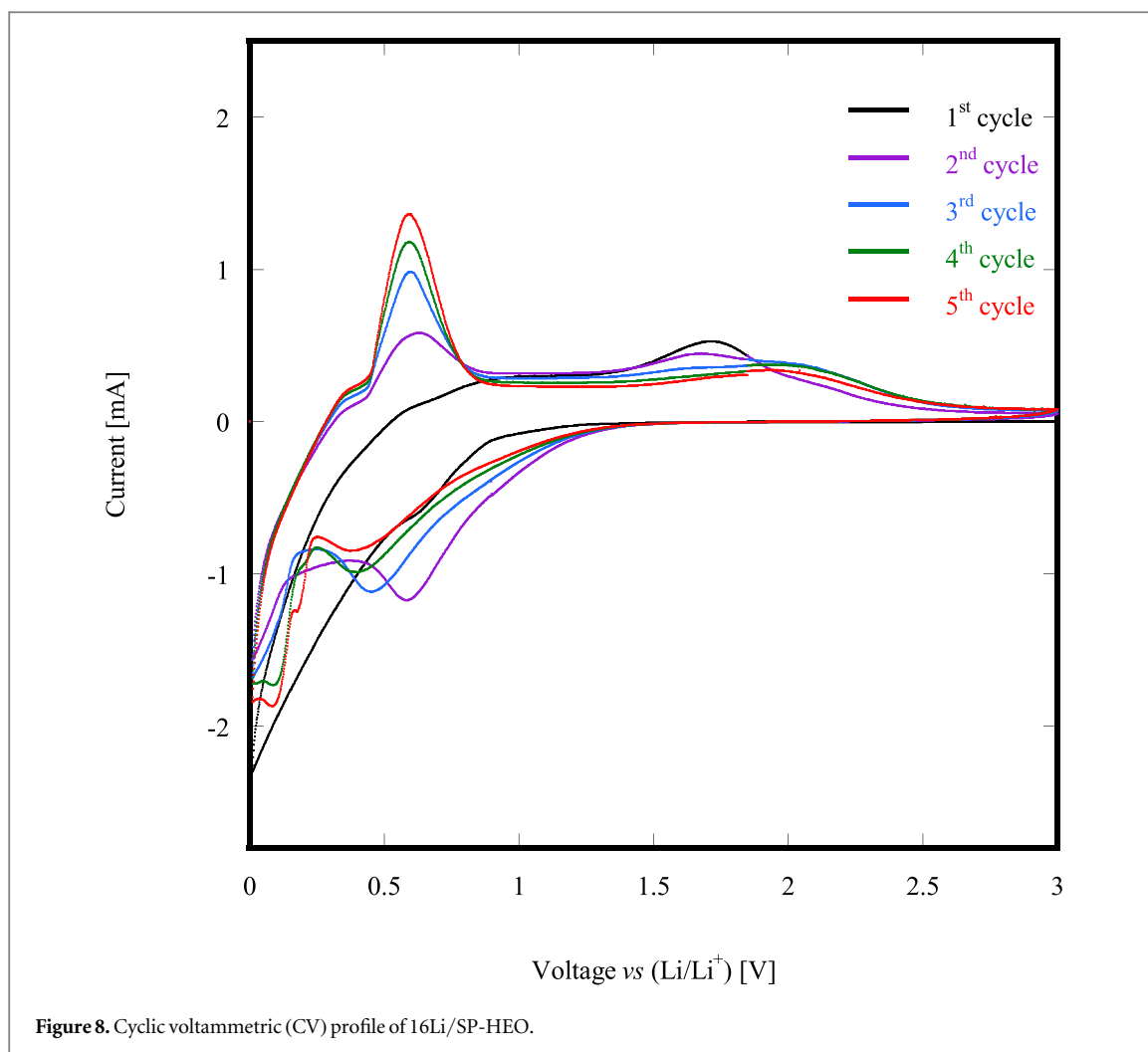
To reveal phase transformations leading to the formation of rock-salt single phase a DTA-TG run of sample 33Li/RS-HEO after the impregnation step was carried out. In figure 6 the corresponding thermograph is shown.

The thermal behavior appears quite complex with the appearance of several endothermic events: the first one ($\alpha - 156^\circ\text{C}$) represents the evolution of adsorbed water (with associated about 20% weigh loss), the second one ($\beta - 257^\circ\text{C}$) represents the melting of LiNO₃ [38]. Besides, there is a progressive and continuous loss of mass, started at 200 °C and ended at about 450 °C, providing an additional 15% weight loss, associated to the evolution of chemically-bonded water from the hydroxides or hydrous oxides formed during the coprecipitation [33]; for this decomposition, occurring in a wide range of temperature, there is no clear endo peak in the thermogram even though a shoulder around 300 °C is present in the DTA signal. Two additional endo events, $\gamma - 490^\circ\text{C}$ and $\delta - 667^\circ\text{C}$, are due to the thermal decomposition of LiNO₃, globally giving rise to an additional 15% of weight loss; indeed γ is the thermal decomposition of molten LiNO₃ to LiNO₂ (and O₂) whereas δ is the decomposition of LiNO₂ to Li₂O and a mixture of N₂, O₂, NO and NO₂ [43]. Eventually, there is a last, sharp endo event, $\lambda - 950^\circ\text{C}$, which can be associated to the transition multiphase-system to rock-salt single phase, according to Spiridigliozzi [38] as no weight loss is associated to this endo event. Indeed, it has been proved [38] that: (i) Li₂O formed by thermal decomposition of LiNO₃ firstly reacts with Co₃O₄ (obtained by natural oxidation of Co-based compound formed during coprecipitation) giving rise to LiCoO₂; (ii) at higher temperature, LiCoO₂ dissolves in the rocksalt structure, when the single phase is formed, according to the following reaction:



Thus Li⁺ occupies octahedral sites so balancing Co³⁺ and Ni³⁺ cations also present in the high entropy rock-salt structure so that no weight loss is associated to the transition multiphase system → single rock-salt phase, unlike occurring in RS HEO without doping with Lithium where a clear weight loss occurs in correspondence of such a transition.

A series of Nuclear Magnetic Resonance (NMR) tests have been developed to characterize the structure of the differently Li-loaded RS-HEO systems. The NMR transition frequencies are strictly related to the electron distribution around the nuclei which can shield them from the applied magnetic field. Thus, 7Li MAS NMR measurements have been used to characterize the Li environments of the Li/RS-HEO series. All the spectra of the RS-HEO doped with different amounts of lithium present one resonance located at about $\delta = -0,4$ [ppm] with a wide spinning sideband pattern. The 1D MAS spectrum indicates the presence of a rocksalt-structured single phase. The recorded spectra, shown in figures 7(a)–(d), indicate that the samples with different Li loadings



have quite different lineshapes, meaning that they have similar lattice parameters but slightly different lithium occupancy.

Moreover, by comparing the Li/RS-HEO series spectra, it is possible to note an irregular shape in the range $(-500; 500)$ [ppm] with increasing peaks per each one around 0 [ppm], meaning that exists a high disorder within the lattice, as expected for high-entropy materials. Carefully analyzing the same range, it is possible to note that the visible peaks vary according to the different Li loadings; in particular, increasing the percentage of Li in the RS-HEO series leads to a reduction of the number of peaks centered around 0 [ppm], that being an indirect confirmation of a reduction of the overall lattice disorder (the more Li is added to the system, the more the other cations are reduced relatively, with the equimolarity being the condition of maximum lattice disorder, i.e. 16Li/RS-HEO).

The maximum resonance peak for each analyzed sample is centered in $\delta = -0,4$ [ppm], being it is relatively sharp and symmetric, indicating that Li occupies octahedral sites of the structure. Besides, it is interesting to note that for samples 33Li/RS-HEO and 41Li/RS-HEO, the left sideband pattern is overlapped with another very small sideband pattern in the region 600-200 ppm (see figures 7(c) and (d), suggesting that a different environment surrounds a small quantity of the whole Li present within the system.

Finally, the RS-HEO series has been referenced to the LiCoO₂ spectrum (figure 7(e)), assessing that all the prepared systems are comparable with it, with the only difference between LiCoO₂ main peak (centered at $\delta = -0,4$ [ppm]) is given by a significantly higher degree of lattice disorder.

3.3. Electrochemical characterization of the cells

Figure 8 shows the Cyclic voltammetric (CV) profile of the 16Li/SP-HEO sample, including the first five cathodic scans at 50 mA/g. The first cycle (black line) only exhibits a negligible peak in correspondence of 1.75 V. The shape of the first cycle has been expected, as it represents the background analysis. Starting from the third cycle, the performed scans are more representative of the electrochemical behavior of the cathode itself, with the registered oxidation reactions (charge phase, i.e. delithiation of the cathode) occurring in the range

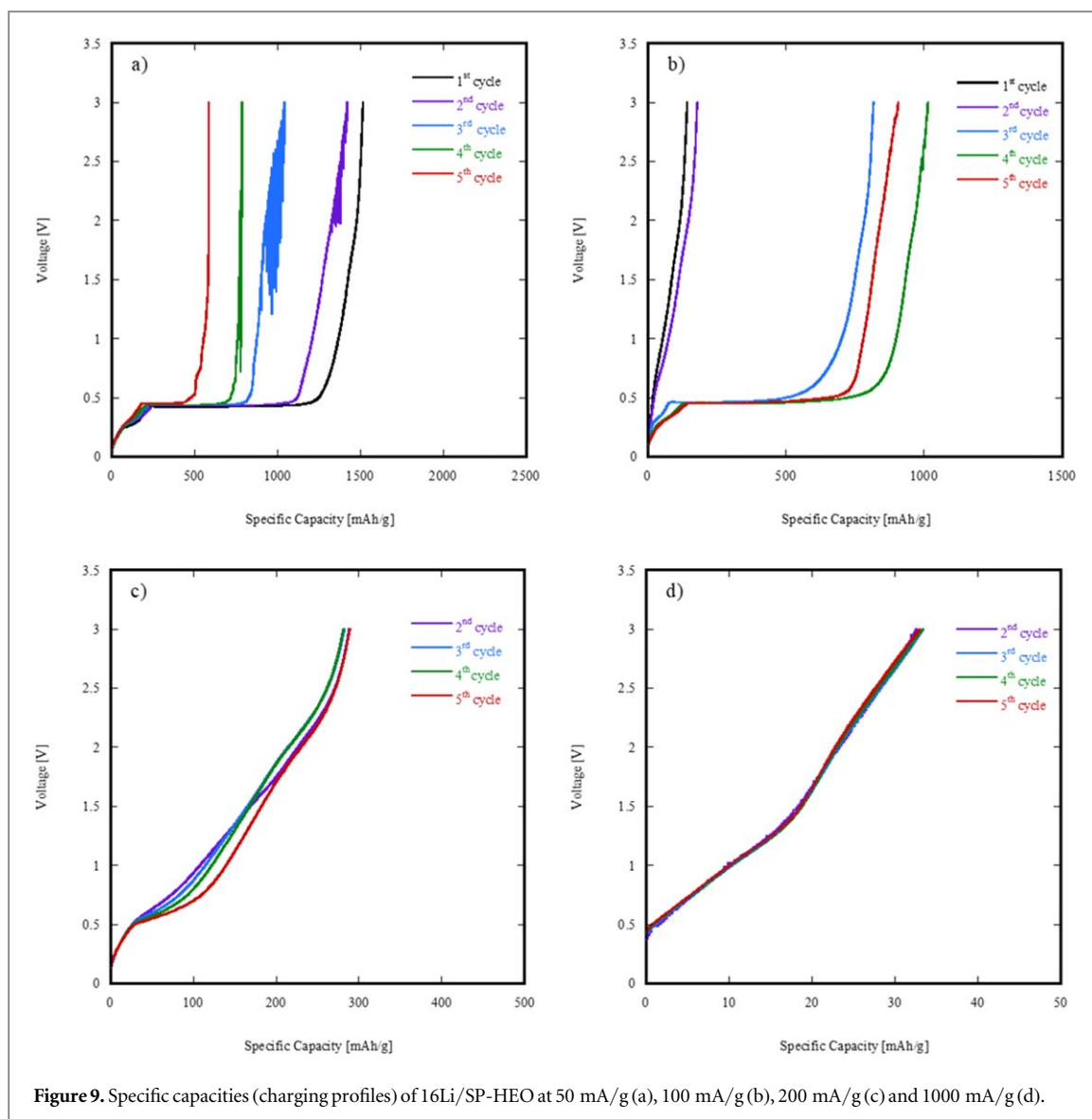


Figure 9. Specific capacities (charging profiles) of 16Li/SP-HEO at 50 mA/g (a), 100 mA/g (b), 200 mA/g (c) and 1000 mA/g (d).

1.6–1.8 V. Such broad peaks very likely identify the oxidation of Fe, Mn and Co within the spinel-like lattice compensating Li^+ losses. Conversely, upon discharge (i.e. lithiation of the cathode) starting from the 3rd cycle, the registered reduction peaks are not symmetrical with the corresponding oxidation ones, occurring at the following potential values: 0.453 V—3rd cycle, 0.399 V—4th cycle, 0.3737 V—5th cycle. Such asymmetry of RedOx peaks of the 16Li/SP-HEO sample indicates a strong irreversibility of the lithiation/delithiation process, as also evidenced in the following.

The sharp oxidation peaks observable in the range 0.7 V – 0.75 V, very likely coupled with the reduction peaks at ~ 0 V, can be attributed to the generation of a solid in the electrolyte interface (SEI) layer and Li_2O [44, 45].

In fact, even though the 16Li/SP-HEO specific capacity reaches a very good value ($\approx 2000 \text{ mAh g}^{-1}$), due to the asymmetry of the lithiation/delithiation process, there is a rapid degradation of the cathode within the whole cell after few charge/discharge cycles, thus leading to a fast capacity fading.

Figure 9(a) shows 16Li/SP-HEO specific capacity (charging profile) at 50 mA g^{-1} , while figures 9(b)–(d) shows 16Li/SP-HEO specific capacity (charging profile) at 100 mA/g , 200 mA/g and 1000 mA g^{-1} , both after five complete cycles.

As the number of complete cycles increases, 16Li/SP-HEO exhibits a large instability, particularly at low specific current conditions (50 mA/g *in primis*), and, consequently, a pronounced capacity fading. In other words, as soon as the sample is tested for the first time, unstable conditions involving very fast Li migration from the cathode up to the anode (probably due to the proneness of many cations of the SP-HEO system to be oxidized) are achieved, as also indicated by the very high capacity registered upon the first 2 cycles ($\approx 1500 \text{ mAh g}^{-1}$). However, since the lithiation reverse process is not symmetric (figure 8(a)), not all the migrated Li is incorporated back into

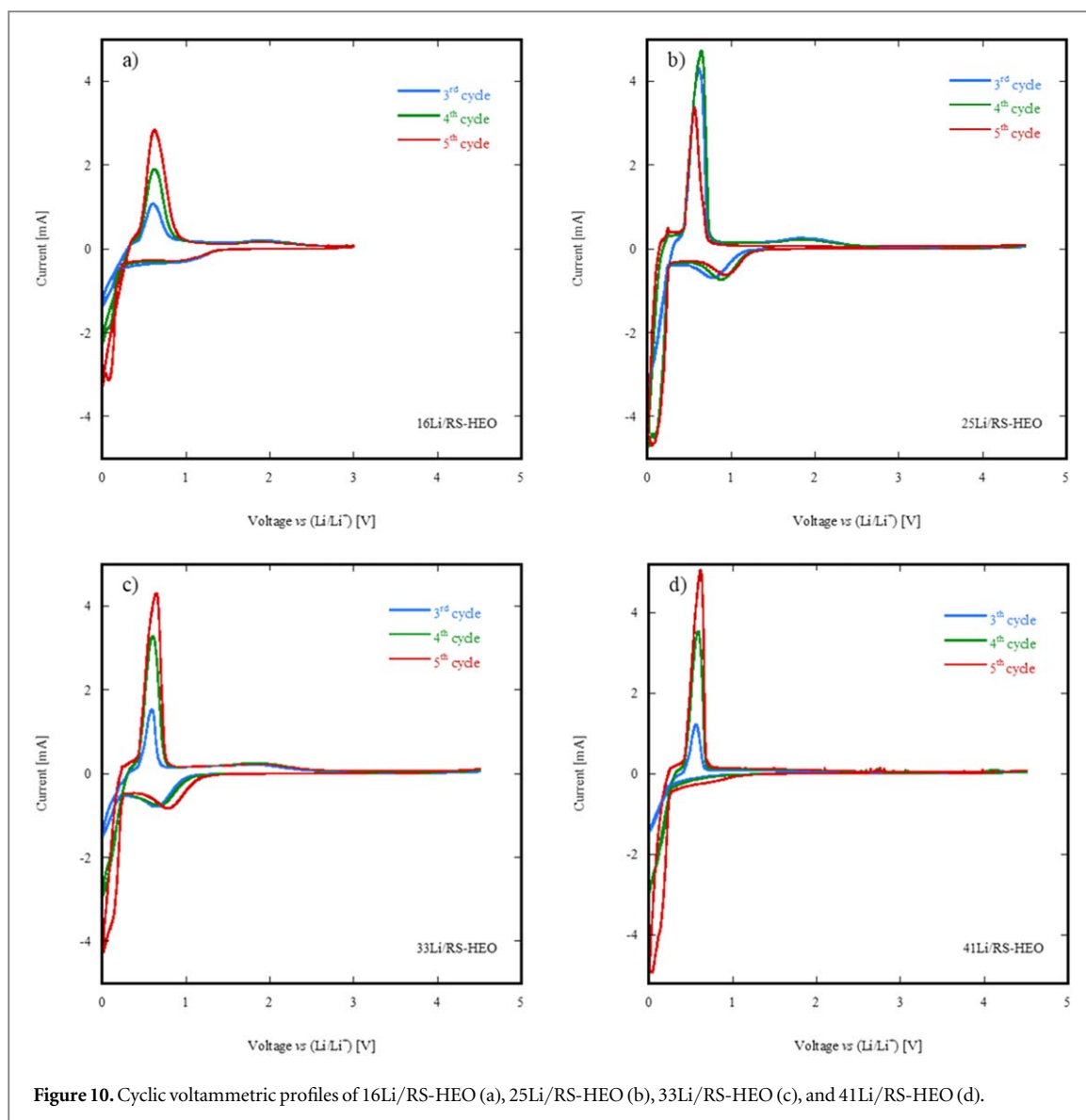


Figure 10. Cyclic voltammetric profiles of 16Li/RS-HEO (a), 25Li/RS-HEO (b), 33Li/RS-HEO (c), and 41Li/RS-HEO (d).

the cathode, thus causing a strongly evident capacity fading of the whole cell. Moreover, such irreversibility of the lithiation/delithiation mechanism is also very likely due to the formation of a solid electrolyte interphase (SEI) layer between the cathodes and the liquid electrolyte, induced by the large amount of Li^+ ions migrating during the very first cycles.

By carefully analyzing the plots in figure 9, it is worth noting that the specific capacity of 16Li/SP-HEO decreases with the increasing of the current density. In particular, at 200 mA g^{-1} , the specific capacity of 16Li/SP-HEO is almost one order of magnitude lower than the one registered at lower current density (i.e. 50 mA g^{-1}), being $\approx 300 \text{ mAh g}^{-1}$. Finally, increasing the current density to 1000 mA/g , 16Li/SP-HEO specific capacity dramatically drops of one order of magnitude more, achieving $\approx 25\text{--}30 \text{ mAh g}^{-1}$ independently from the considered cycle. In other words, at high current densities 16Li/SP-HEO lithiation/delithiation mechanism becomes highly stable but to the detriment of its overall specific capacity, not being of practical interest as a substitute cathode for Li-ion batteries.

A possible explanation of this behavior is strictly related to the RedOx reactions occurring upon 16Li/SP-HEO lithiation/delithiation, as higher current densities (i.e. faster cell charge/discharge cycles) globally inhibit such reactions in favor of moving in absolute terms very low quantities of Li^+ ions, related to the very low registered capacities. Conversely, at lower current densities, the highly disordered structure of 16Li/SP-HEO, as the proneness of the different cations to be oxidized upon cathode's delithiation, contribute to move globally high quantities of Li^+ ions but, in turn, induce a strong irreversibility of the overall process, possibly involving a structural collapse during the first discharge cycles, leading to an unacceptable capacity fading upon very few charge/discharge cycles.

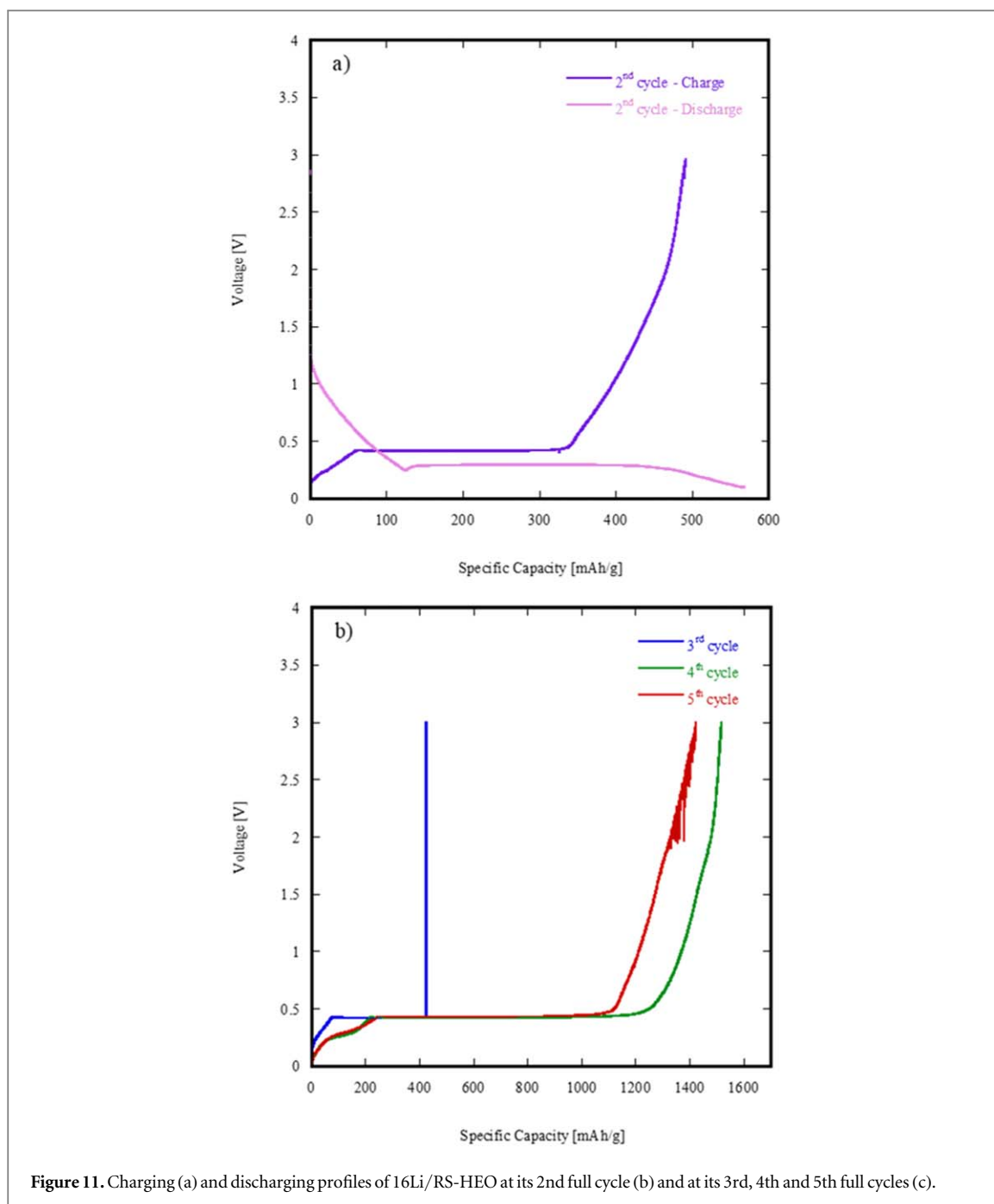


Figure 11. Charging (a) and discharging profiles of 16Li/RS-HEO at its 2nd full cycle (b) and at its 3rd, 4th and 5th full cycles (c).

In order to investigate the Li loading effect on the reactions and kinetics of RS-HEO cathodes, cyclic voltammetric tests have been carried out on the Li/RS-HEO series samples. Figure 10 shows the Cyclic voltammetric (CV) profiles of the Li/RS-HEO series, i.e. 16Li/RS-HEO, 25Li/RS-HEO, 33Li/RS-HEO, and 41Li/RS-HEO samples, including the 3rd, 4th and 5th cathodic scans at 50 mA g^{-1} , as the 1st and 2nd cycles exhibited the same features of 16Li/SP-HEO, thus not representing a stable testing condition.

All the registered profiles in figure 10 display clear oxidation and reduction peaks, even though with several interesting differences between the various samples. In particular, for each tested cathode, it is always possible to identify a sharp oxidation peak centered in the range between $0.5 \text{ V} - 0.6 \text{ V}$ (versus Li/Li⁺) and at least one reduction peak at lower voltages. For each tested cathode, a major reduction peak is observable at values close to zero as potential and negative values for currents. Additionally, 25Li/RS-HEO and 33Li/RS-HEO exhibit visible secondary peaks at positive potentials, i.e. $0.5 \text{ V} < x < 0.65 \text{ V}$ (versus Li/Li⁺), thus indicating that the lithiation process occurs along with the formation of a SEI layer and/or of Li₂O, as similarly observed in the 16Li/SP-HEO.

Moreover, by analyzing the peak shapes and positions, a higher symmetry of the lithiation/delithiation mechanism compared to SP-HEO suggests a definitely greater reversibility of the overall process in the Li/RS-

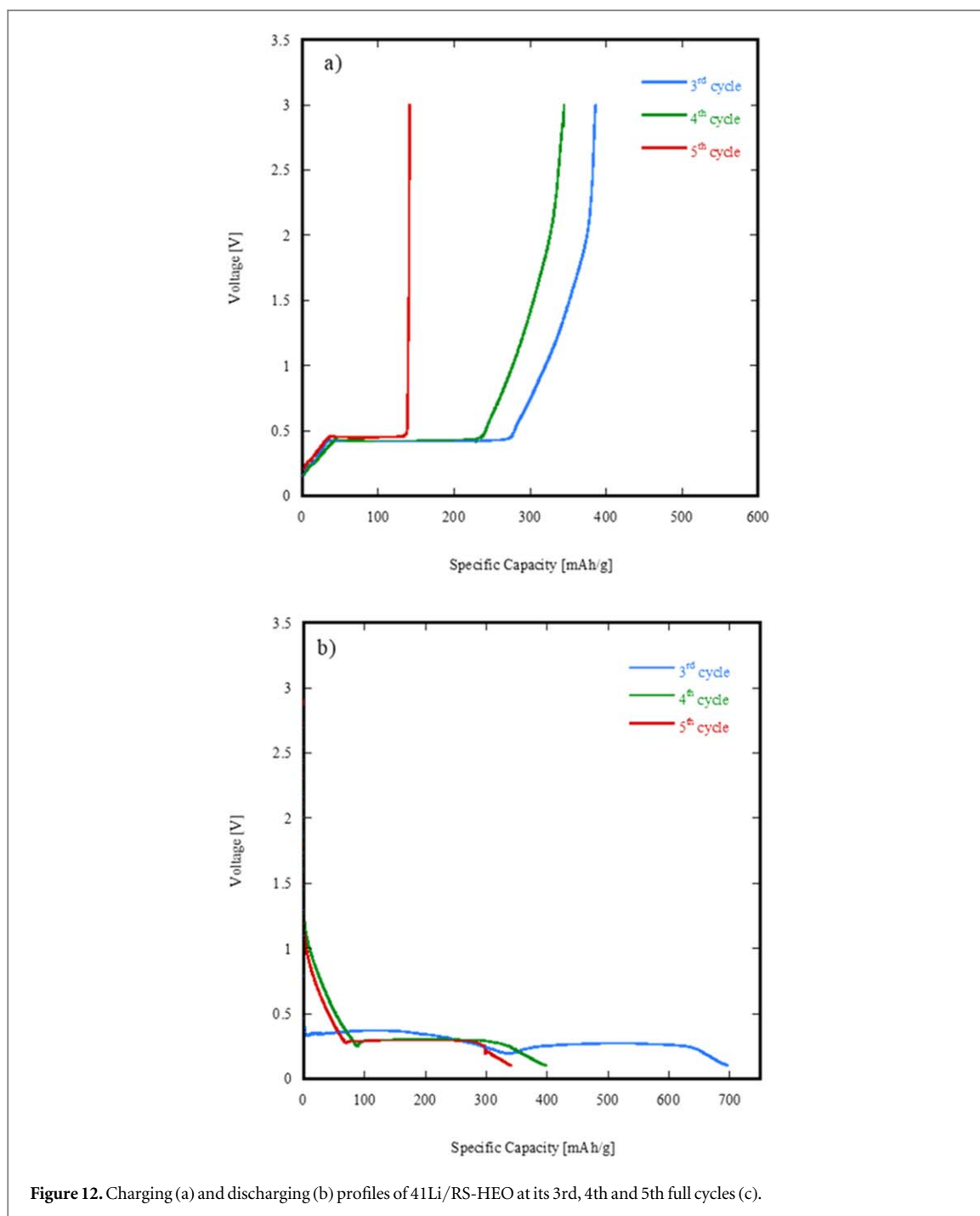


Figure 12. Charging (a) and discharging (b) profiles of 41Li/RS-HEO at its 3rd, 4th and 5th full cycles (c).

HEO series of samples (with the 25 Li/RS-HEO sample exhibiting the most pronounced symmetry, with an oxidation peak at 0.58 V and two reduction peak at 0.93 V and 0.01 V for all the investigated cycles). According to different Li loadings, the various Li/RS-HEO cathodes own different cycle hysteresis: lower Li loading is related to greater cycle hysteresis and *viceversa*. Moreover, it can be noted that the RedOx reactions occur much more easily in cathodes with lower Li loadings, as for 41Li/RS-HEO a current of almost 5 mA is required to activate the lithiation/delithiation mechanism, contrarily to 16Li-RS-HEO that required just about 2 mA in each investigated cycle. Such behavior could be related to what has been observed via NMR, i.e. the presence of possible short-range ordered for Li⁺ ions within the rocksalt lattice of 41Li/RS-HEO (possibly involving the presence of Li₂O domains) that is an unfavorable factor for the reaction kinetics thus determining the high currents demanded for the oxidation/reduction of the involved species.

Finally, the oxidation and main reduction peaks potential, being very low compared to the Li/Li⁺ reference reaction, suggests that all the Li/RS-HEO samples have a fast Li ion transfer rate upon all the reaction process.

To evaluate their specific capacities and cycling stability, full cells with the Li/RS-HEO series of cathodes were cyclically charged/discharged at a constant current ($C/20$). Primarily, each cell is first rested for 30 min, subsequently charged at a constant current rate for 20 h, and held in stationary condition at the upper voltage limit. At last, the cell is discharged at a constant current rate to the lower voltage limit for 20 h.

Figure 11(a) shows the charging and discharging profiles of 16Li/RS-HEO at its 2nd full cycle (the first is omitted as possibly influenced by non-stationary conditions).

By firstly analyzing the 16Li/RS-HEO charging profile, the full cell charging process starts from approximately 0.45 V, reaching an upper voltage threshold of around 2.96 V, which corresponds to a specific capacity of almost 500 mAh/g.

After the rest from the charging phase, cell starts to discharge from the upper limit voltage, reaching the lower voltage threshold (i.e. 0.25 V) in 4 h.

Figure 12(b) shows the charging profiles of 16Li/RS-HEO at its 3rd, 4th and 5th full cycles (i.e. right after the full cycle shown in figure 12(a)). From such profiles, a significant instability of the 16Li/RS-HEO specific capacity over full charging cycles is highly noticeable, achieving an outstanding value of almost 1500 mAh g^{-1} in the 3rd cycle.

The great variation observed in the specific capacities of 16Li/RS-HEO could be related to the broad reduction peak upon lithiation observed in figure 8, very likely involving a continuous and disordered reduction of the RS-HEO cations, as recently reported in similar systems [33].

Confirming the cyclic voltammetry results, Li/RS-HEO samples with higher Li loadings exhibited relatively higher cycling stability (even though a not negligible capacity fading is still observable, with a minimum of 12,5% capacity loss per cycle for the 41Li/RS-HEO sample), at the expense of lower specific capacities (up to slightly more than 300 mA/g for the 41Li/RS-HEO sample).

We attributed such behavior (i.e. when the Li ratio in the RS/HEO cathodes increases, the specific capacity decreases) to the decreasing ratio between transition metal cations and lithium ions within the system, resulting in fewer redox reactions occurring within the cell upon the lithiation/delithiation process. In other words, as for each synthesized system, we fixed the sum of the molar fractions of the 6 involved cations; an increasing Li content led to a decrease of the sum of the other 5 cations, among which the ones owning the redox behaviour needed to counterbalance Li ions intercalation/deintercalation.

Such results are evident from figure 12, exemplarily showing the charging and discharging profiles of 41Li/RS-HEO at its 3rd, 4th and 5th full cycles.

Very likely, the structural collapse of the variously prepared Li-HEO cathodes after few cycles is primarily due to their chemical composition (abundant in Li-loadings), the formation of lithium oxide at the electrolyte interface, and the inherent lattice disorder. Li-HEOs' high configurational entropy, while contributing to initial capacity and performance benefits due to a more accessible 3D intercalation pattern for lithium ions, also renders these materials structurally unstable already in the short term (i.e. after very few charge/discharge cycles). The abundant extraction of lithium ions (as highlighted by the very high specific capacities upon the first 2–3 cycles) hinder the overall material's stability, leading to structural collapse. Additionally, the formation of lithium oxide during the initial cycles further hinders the reversibility of the charging process and contributes to the observed fast degradation of the electrode's structure.

4. Conclusion

In the present study, two differently structured HEOs have been synthesized via co-precipitation and subsequently impregnated with different Li loadings, aiming to evaluate their electrochemical performances as potential cathodes for LIBs.

Cyclic voltammetry experiments showed different electrochemical responses in relation to different Li host structures (either rocksalt-like or spinel-like) and to different lithium loadings. The observed results showed broad and strongly irreversible hysteresis cycles for the Li/SP-HEO sample, whilst thin and narrow hysteresis cycles (correlated to increased lithium loadings) for Li/RS-HEO series of samples, with single oxidation peaks centered between 0.5 V and 0.7 V and multiple reduction peaks depending on different lithium loadings. High lithium loadings led to the disappearance of the secondary reduction peak upon the lithiation process, causing an imbalance in the cell's oxidation reaction and instability.

Moreover, it has been noted that as lithium content in the RS-HEO system increased, the overall cell cycling stability degraded. This behavior was very likely due to the decreasing ratio between transition metal cations and lithium ions, resulting in fewer redox reactions occurring within the cell upon the lithiation/delithiation process.

However, despite the observed cycling instability for most of the tested samples, increasing lithium loadings positively affected the cell capacity, even though a significant capacity fading occurs under high current rates,

very likely due to the abundant extraction of lithium ions upon the first charge/discharge cycles that hinder the overall material's stability, subsequently leading to a fast structural collapse.

Definitely, Li-doped rocksalt structured high entropy materials are promising for their application as LIBs cathodes in terms of high specific capacities, even though stability issues at medium and high current densities suggest a quick degradation and fast charge/discharge cycles. The observed complex interplay of factors affecting the variously tested samples needs further research to optimize Li-rich HEO compositions and structural design to balance the unique properties of HEO structures with the need for stability and durability in LIB cathodes.

Data availability statement

The data cannot be made publicly available upon publication because they are owned by a third party and the terms of use prevent public distribution. The data that support the findings of this study are available upon reasonable request from the authors.

ORCID iDs

Gianfranco Dell'Agli  <https://orcid.org/0000-0001-7690-846X>

References

- [1] Yeh J W, Chen S K, Lin S J, Gan J Y, Chin T S, Shun T T, Tsau C H and Chang S Y 2004 Nanostructured high-entropy alloys with multiple principal elements: novel alloy design concepts and outcomes *Adv. Eng. Mater.* **6** 299–303
- [2] Huang P K, Yeh J W, Shun T T and Chen S K 2004 Multi-principal-element alloys with improved oxidation and wear resistance for thermal spray coating *Adv. Eng. Mater.* **6** 74–8
- [3] Rost C M, Sacht E, Borman T, Moballegh A, Dickey E C, Hou D, Jones J L, Curtarolo S and Maria J P 2015 Entropy-stabilized oxides *Nat. Commun.* **6** 8485
- [4] Spiridigliozzi L, Ferone C, Cioffi R, Accardo G, Frattini D and Dell'Agli G 2020 Entropy-stabilized oxides owning fluorite structure obtained by hydrothermal treatment *Materials* **13** 558
- [5] Jiang S, Hu T, Gild J, Zhou N, Nie J, Qin M, Harrington T, Vecchio K and Luo J 2018 A new class of high-entropy perovskite oxides *Scripta Mater.* **142** 116–20
- [6] Zhou J, Zhang J, Zhang F, Niu B, Le L and Wang W 2018 High-entropy carbide: a novel class of multicomponent ceramics *Ceram. Int.* **44** 22014–8
- [7] Sun Z, Zhao Y, Sun C, Ni Q, Wang C and Jin H 2022 High entropy spinel-structure oxide for electrochemical application *Chem. Eng. J.* **431** 133448
- [8] Gild J, Braun J, Kaufmann K, Marin E, Harrington T, Hopkins P, Vecchio K and Luo J 2019 A high-entropy silicide: $(\text{Mo}_{0.2}\text{Nb}_{0.2}\text{Ta}_{0.2}\text{Ti}_{0.2}\text{W}_{0.2})\text{Si}_2$ *J. Materiomics* **5** 337–43
- [9] Sun Y and Dai S 2021 High-entropy materials for catalysis: a new frontier *Sci. Adv.* **7** eabg1600
- [10] Fu M, Ma X, Zhao K, Li X and Su D 2021 High-entropy materials for energy-related applications *Science* **24** 102177
- [11] Bérardan D, Franger S, Meena A K and Dragoë N 2016 Room temperature lithium superionic conductivity in high entropy oxides *J. Mater. Chem.* **4** 9536–41
- [12] Sarkar A, Kruk R and Hahn H 2019 Magnetic properties of high entropy oxides *Dalton Trans.* **50** 1973–82
- [13] Zhao Y, Li H, Zu Y, Wang Y, Fu X, Zhou W and Chen G 2023 MgCoNiCuZn)O with particular microstructure and distinctive electrochemical performance prepared using ultrafast high-temperature sintering *J. Eur. Ceram. Soc.* **43** 7573–80
- [14] Spiridigliozzi L, Dell'Agli G, Esposito S, Rivolo P, Grasso S, Sglavo V M and Biesuz M 2022 Ultra-fast high-temperature sintering (UHS) of $\text{Ce}_{0.2}\text{Zr}_{0.2}\text{Y}_{0.2}\text{Gd}_{0.2}\text{La}_{0.2}\text{O}_{2-\delta}$ fluorite-structured entropy-stabilized oxide (F-ESO) *Scripta Mater.* **214** 114655
- [15] Li H et al 2021 High-entropy oxides: advanced research on electrical properties *Coatings* **11** 628
- [16] Guo H X, Wang W M, He C Y, Liu B H, Yu D M, Liu G and Gao X H 2021 Entropy-assisted high-entropy oxide with a spinel structure toward high-temperature infrared radiation materials *ACS Appl. Mater. Interfaces* **14** 1950–60
- [17] Xu L, Wang H, Su L, Lu D, Peng K and Gao H 2021 A new class of high-entropy fluorite oxides with tunable expansion coefficients, low thermal conductivity and exceptional sintering resistance *J. Eur. Ceram. Soc.* **41** 6670–6
- [18] Li F, Zhou L, Liu J X, Liang Y and Zhang G J 2019 High-entropy pyrochlores with low thermal conductivity for thermal barrier coating materials *J. Adv. Ceram.* **8** 576–82
- [19] Xu Y, Xu X and Bi L 2022 A high-entropy spinel ceramic oxide as the cathode for proton-conducting solid oxide fuel cells *J. Adv. Ceram.* **11** 794–804
- [20] Liu Z Y, Liu Y, Xu Y, Zhang H, Shao Z, Wang Z and Chen H 2023 Novel high-entropy oxides for energy storage and conversion: from fundamentals to practical applications *Green Energy & Environment* **8** 1341–57
- [21] Chen Y, Fu H, Huang Y, Huang L, Zheng X, Dai Y, Huang Y and Luo W 2020 Opportunities for high-entropy materials in rechargeable batteries *ACS Mater. Lett.* **3** 160–70
- [22] Raza H, Bai S, Cheng J, Majumder S, Zhu H, Liu Q and Chen G 2023 Li-S batteries: challenges, achievements and opportunities *Electrochemical Energy Reviews* **6** 29
- [23] Xu J, Cai X, Cai S, Shao Y, Hu C, Lu S and Ding S 2023 High-energy lithium-ion batteries: recent progress and a promising future in applications *Energy & Environmental Materials* **6** e12450
- [24] Raza H et al 2022 Low-temperature calcination of metal-organic frameworks (MOFs) to derive the high entropy stabilized oxide for high performance lithium-sulfur batteries *ECS Meeting Abstracts* **MA2022-01** 2432
- [25] Zheng Y, Wu X, Lan X and Hu R 2021 A spinel $(\text{FeNiCrMnMgAl})_3\text{O}_4$ high entropy oxide as a cycling stable anode material for Li-ion batteries *Processes* **10** 49

- [26] Duan C, Tian K, Li X, Wang D, Sun H, Zheng R, Wang Z and Liu Y 2021 New spinel high-entropy oxides (FeCoNiCrMnXLi)₃O₄ (X = Cu, Mg, Zn) as the anode material for lithium-ion batteries *Ceram. Int.* **47** 32025–32
- [27] Cui Y et al 2022 High entropy fluorides as conversion cathodes with tailorable electrochemical performance *J Energy Chem.* **72** 342–51
- [28] Wang K et al 2023 Synergy of cations in high entropy oxide lithium ion battery anode *Nat. Commun.* **14** 1487
- [29] Qiu N, Chen H, Yang Z, Sun S, Wang Y and Cui Y 2019 A high entropy oxide (Mg_{0.2}Co_{0.2}Ni_{0.2}Cu_{0.2}Zn_{0.2}O) with superior lithium storage performance *J. Alloys Compd.* **777** 767–74
- [30] Wang X L, Jin E M, Sahoo G and Jeong S M 2023 High-entropy metal oxide (NiMnCrCoFe)₃O₄ anode materials with controlled morphology for high-performance lithium-ion batteries *Batteries* **9** 147
- [31] Zou X, Zhang Y R, Huang Z P, Yue K and Guo Z H 2023 High-entropy oxides: an emerging anode material for lithium-ion batteries *Chem. Commun.* **59** 13535–50
- [32] Hou S, Su L, Wang S, Cui Y, Cao J, Min H and Xu F 2023 Unlocking the origins of highly reversible lithium storage and stable cycling in a spinel high-entropy oxide anode for lithium-ion batteries. *Adv. Funct. Mater.* **34** 2307923
- [33] Biesuz M, Spiridigliozi L, Dell'Agli G, Bortolotti M and Sglavo V M 2018 Synthesis and sintering of (Mg, Co, Ni, Cu, Zn) O entropy-stabilized oxides obtained by wet chemical methods *J. Mater. Sci.* **53** 8074–85
- [34] Turco R et al 2020 Active and stable ceria-zirconia supported molybdenum oxide catalysts for cyclooctene epoxidation: Effect of the preparation procedure *Catal. Today* **345** 201–12
- [35] Spiridigliozi L, Di Bartolomeo E, Dell'Agli G and Zurlo F 2020 GDC-based infiltrated electrodes for solid oxide electrolyzer cells (SOECs) *Appl. Sci.* **10** 3882
- [36] Jiang S P 2006 A review of wet impregnation—an alternative method for the fabrication of high-performance and nano-structured electrodes of solid oxide fuel cells *Mater. Sci. Eng.* **418** 199–210
- [37] Liu Z, Liu B, Ding D, Liu M, Chen F and Xia C 2013 Fabrication and modification of solid oxide fuel cell anodes via wet impregnation/infiltration technique *J. Power Sources* **237** 243–59
- [38] Spiridigliozi L, Dell'Agli G, Callone E, Dirè S, Campostrini R, Bettotti P, Bortolotti M, Speranza G, Sglavo V M and Biesuz M 2022 A structural and thermal investigation of Li-doped high entropy (Mg, Co, Ni, Cu, Zn) O obtained by co-precipitation *J. Alloys Compd.* **927** 166933
- [39] Sarkar A, Eggert B, Witte R, Lill J, Velasco L, Wang Q and Kruk R 2022 Comprehensive investigation of crystallographic, spin-electronic and magnetic structure of (Co_{0.2}Cr_{0.2}Fe_{0.2}Mn_{0.2}Ni_{0.2})₃O₄: unraveling the suppression of configuration entropy in high entropy oxides *Acta Mater.* **226** 117581
- [40] Holland T J B and Redfern S A T 1997 Unit cell refinement from powder diffraction data: the use of regression diagnostics *Mineral. Mag.* **61** 65–77
- [41] Spiridigliozi L, Dell'Agli G, Biesuz M, Sglavo V M and Pansini M 2016 Effect of the precipitating agent on the synthesis and sintering behavior of 20 mol Sm-doped ceria *Adv. Mater. Sci. Eng.* **2016** 6096123
- [42] Raza H, Cheng J, Lin C, Majumder S, Zheng G and Chen G 2023 High-entropy stabilized oxides derived via a low-temperature template route for high-performance lithium-sulfur batteries *EcoMat* **5** e12324
- [43] Mohammad M B, Brooks G A and Rhamdhani M A 2018 Premelting, melting, and degradation properties of molten alkali nitrates: LiNO₃, NaNO₃, KNO₃, and binary NaNO₃-KNO₃ *Metall. Mater. Trans. B* **49** 1482–98
- [44] Jin C, Wang Z, Luo C, Qin C, Li Y and Wang Z 2023 Dealloyed porous NiFe₂O₄/NiO with Dual-network structure as high-performance anodes for lithium-ion batteries *Int. J. Mol. Sci.* **24** 4152
- [45] Yao L H, Zhao J G, Pan Q L, Li X Y, Xing B Y, Jiang S, Song J and Pang M J 2022 Tailoring NiO@NiFe₂O₄/CNTs triphase hybrids towards high-performance anode for lithium-ion batteries *J. Alloys Compd.* **912** 165209